ELSEVIER

Journal of Nuclear Materials 318 (2003) 185–191

journal of nuclear materials

www.elsevier.com/locate/jnucmat

Characterization of lead–bismuth eutectic target material for accelerator driven transmuters

Yousry Gohar *

Argonne National Laboratory, Fusion Power Program Technology Development Division, 9700 South Cass Avenue, Argonne, IL 60439, USA

Abstract

Lead–bismuth eutectic (LBE) is under consideration as a target material with high-energy protons for generating neutrons to drive actinide and fission product transmuters. A characterization has been performed to study the performance of this target material as a function of the main variables and the design selections. The characterization includes the neutron yield, the spatial energy deposition, the neutron spectrum, the beam window performance, and the target buffer requirements. The characterization has also considered high-energy deuteron particles to study the impact on the target neutronic performance. The obtained results quantify the LBE target material performance with proton or deuteron particles as a function of the target variables and selections.

1. Introduction

Lead–bismuth eutectic (LBE) technology is being developed worldwide for spallation neutron targets, which will drive subcritical transmuters [1–4]. This paper is intended to characterize the LBE target material performance including the impact of the main variables and the design selections. The charged particle energy, the target buffer thickness, and the charged particle type are considered in the characterization. The performance analysis includes the neutron yield, the neutron utilization fraction, the neutron spatial distribution, the neutron spectrum, the energy deposition per generated neutron, the beam window nuclear responses, the window operating life, and the nuclear responses in the structural material outside the target buffer. The analysis was performed for proton and deuteron charged particles to define the impact on the LBE material performance. In the analysis process, heat transfer, hydraulics, beam window stresses, and target engineering issues have been considered to insure that the obtained performance is achievable for the LBE target designs.

This work was performed using the spallation target design of the subcritical multiplier (SCM) of the accelerator driven test facility (ADTF) [4–6]. The ADTF is a nuclear research facility that will provide multiple testing and production capabilities. The ADTF target design is based on a coaxial geometrical configuration to satisfy the SCM configuration for minimizing the space requirements and to maximize the SCM utilization of the target neutrons. The target is installed vertically along the SCM axis. LBE is the target material and the target coolant. Ferritic steel (HT-9, Fe–12Cr–1Mo alloy) is the structural material for the target. The target coolant channels and the proton beam are entered vertically from the top above the SCM. The geometrical configuration shown in Fig. 1 has been carefully designed to ensure flow stability and adequate cooling for the beam window and the structural material. The proton beam has a uniform spatial distribution over an 8-cm circular cross-section. The beam tube has 10-cm radius to accommodate the halo current. A hemi-spherical geometry is used for the beam window, which is connected to the beam tube. The beam tube is enclosed inside two coaxial tubes to provide inlet and outlet channels (manifolds) for the LBE coolant. In addition, the materials (LBE and target structure) between the beam trajectory and the boundary of the SCM (buffer)

* Tel.: +1-630 252 4816; fax: +1-630 252 5287.
E-mail address: gohar@anl.gov (Y. Gohar).

0022-3115/03/$ - see front matter
doi:10.1016/S0022-3115(03)00012-6

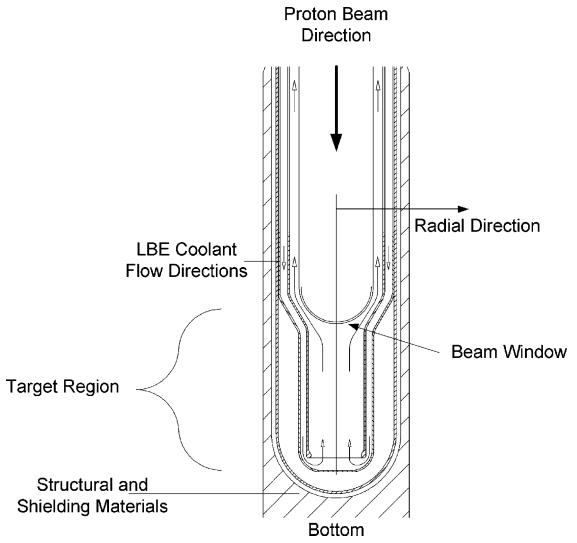

Fig. 1. Lead–bismuth target design concept.

reduce the nuclear responses in the SCM structural material. The utilization of the LBE as a target, buffer, and coolant material does simplify the design. The target and beam configurations of the ADTF were adopted for the work presented in this paper.

The MCNPX code [7] was used to perform the physics analysis of this paper. Each the MCNPX calculation used adequate source sampling in the range of 250 000 to 1 000 000 source particles to achieve statistical error less than 1% within one standard deviation. The characterization results are presented as well as the main conclusions from the analysis. The paper defines the design parameter values to operate the LBE material in spallation targets with a satisfactory performance. Also, recommendations are obtained to maximize the neutron utilization and protect the structural material outside the target buffer from the charged particles and the high-energy neutrons.

2. Energy deposition

The first step in the analysis was to define the energy deposition profile in the LBE for different proton energies. The proton energy considered is in the range of 200–1000 MeV. The results are shown in Fig. 2, which are normalized to the incident proton current density. The peak energy deposition does not occur at the LBE surface but it is inside the LBE material along the beam axis. Such behavior is desirable because the beam window is not exposed to the peak heating value. Also, it does simplify the LBE heat removal. Increasing the charged particle energy reduces the peak power density and spreads the energy deposition in the lead–bismuth. As the proton energy increases above 600 MeV, the peak

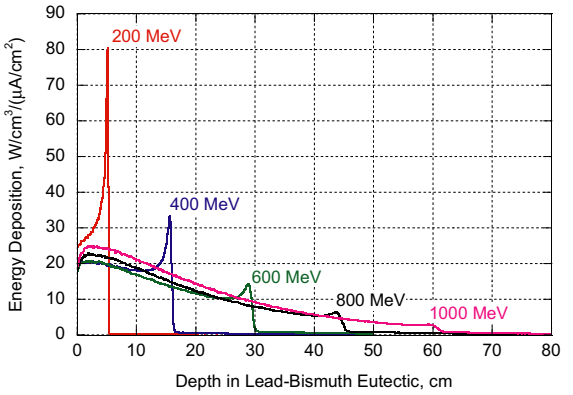

Fig. 2. Spatial energy deposition in the LBE for different proton energies with a uniform beam distribution normalized to the proton beam current density.

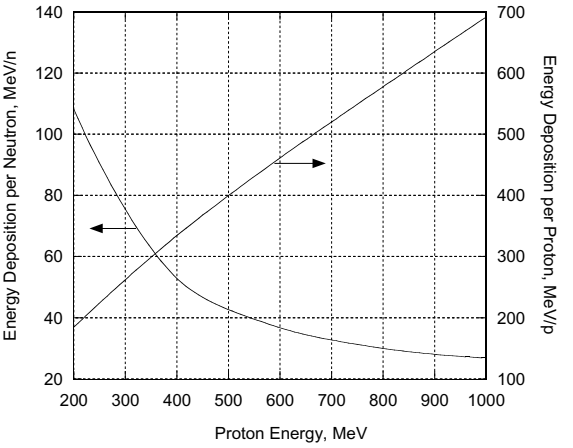

Fig. 3. Energy deposition as a function of the proton energy normalized per incident proton on the right axis and per generated neutron on the left axis.

value shifts from the end of proton beam range to the beam entry area, at about 1 cm from the surface.

The total energy deposition increases linearly as the proton energy increases. However, the energy loss percentage to the endothermic reactions increases as the proton energy increases. The energy deposition per generated neutron shows a very fast decrease with the proton energy up to about 500 MeV, and then it slows down as shown in Fig. 3. Such behavior encourages the use of high-energy protons to reduce the target cooling requirements for specific neutron source strength.

3. Neutron yield

The total number of generated neutrons per proton increases as the proton energy increases as shown in Fig.

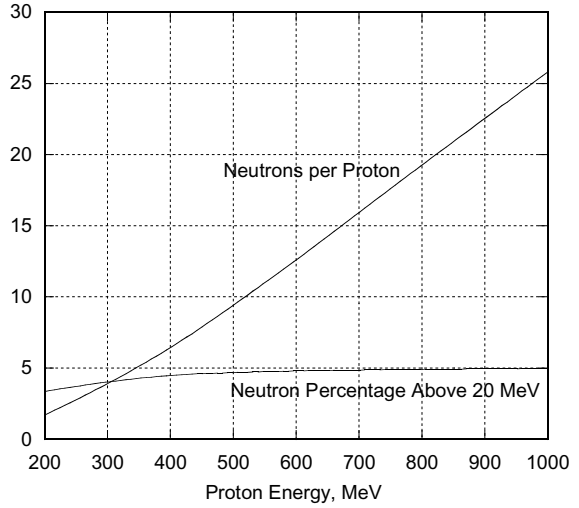

Fig. 4. Number of neutrons per proton and neutron percentage with energy above 20 MeV as a function of the proton energy.

4. This number includes the spallation neutrons and the secondary neutrons from the interactions of the high energy spallation neutrons with the LBE target material. Above 500 MeV proton energy, the number of generated neutrons per proton increases linearly with the proton energy. However, the neutron fraction with energy above 20 MeV reaches a saturation value of ~0.05 as the proton energy increases, as shown in Fig. 4. The neutron utilization fraction is defined as the neutron fraction of the total generated neutrons that does not leave the target region in the beam direction because these neutrons have the opportunity to perform material transmutation. The neutrons leaving the target region in the beam direction will interact with the shield, the reflector, or the transmuter structural material at the bottom of the target region or travel in the beam tube above the target region. The neutron utilization fraction changes from 0.53 at 200 MeV to 0.81 at 1000 MeV proton energy. As the proton energy increases, the neutrons are generated further away from the LBE surface, which increases the radial neutron leakage and subsequently the neutron utilization factor. The generated neutrons leaving the target region in the different directions (top, radial, and bottom) are shown in Fig. 5. In this analysis, an adequate target length is included to slow down, multiply, and reflect the high-energy neutrons at the end of the proton range (referred to as the bottom section). This enhances the neutron production per proton and the neutron utilization fraction. Also, a fixed buffer thickness of 7 cm of LBE material is used in the analyses to protect the structural material of the SCM outside the target region and to function as input/output coolant channels for the LBE target material as shown in Fig. 1. The effect of the buffer thickness on the neutron utilization fraction is discussed later. Again, these results show that the use of high-energy proton is beneficial for enhancing the neutron yield as well as the neutron utilization factor.

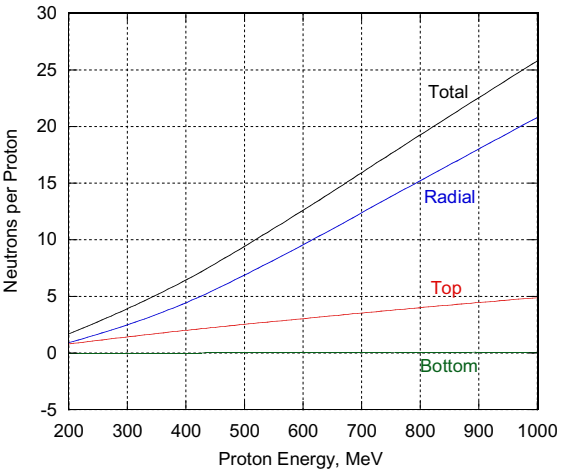

Fig. 5. Generated neutron spatial distribution at the target boundaries as a function of the proton energy.

4. Generated neutron spatial distribution

In the transmuter design, axial power peaking is a design issue, which has a significant impact on the transmuter performance. The spatial distribution of the generated neutrons has a direct impact on the power peaking in the driven systems. It is desirable to distribute

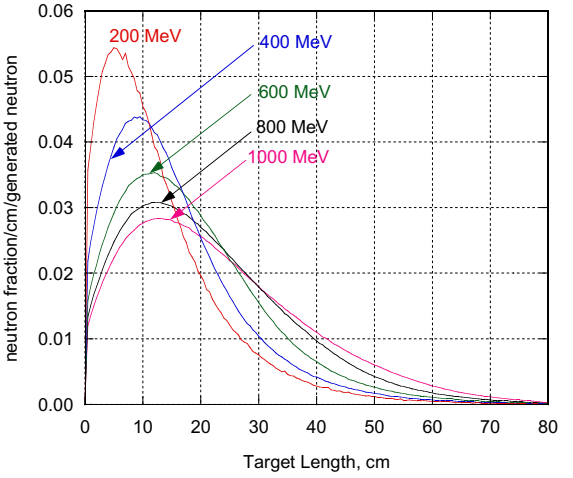

Fig. 6. Generated neutron distribution along the target buffer outer surface for different proton energies normalized per generated neutron.

uniformly the generated neutrons in the transmuter axial direction (beam direction) to reduce the power peaking. The spatial distribution of the generated neutron was calculated at the outer surface of the 7-cm buffer for different proton energies as shown in Fig. 6 per generated neutron. The results show that the uniformity of the generated neutron distribution in the beam direction improves as the proton energy increases. The neutron peak is reduced by a factor of two as the proton energy increases from 200 to 1000 MeV. Also, the neutron peak is shifted further by about 8 cm along the beam direction and the neutron spatial distribution spreads further along the beam axis. These results show that the use of high-energy proton help reducing the axial power peaking in the driven transmuters.

5. Generated neutron spectrum

The generated neutron spectra $n(E)$ at the outer buffer surface for different proton energies are shown in Fig. 7. It should be noted that $n(E)$ is defined as the neutron fraction with energy E MeV per unit energy (MeV) interval normalized per generated neutron. The small wiggles in the neutron spectra between 0.045 and 0.075 MeV are due to the LBE resonance cross-sections in this energy range. The neutron spectra are very similar up to 80 MeV. Above 80 MeV, the neutron density is reduced by a factor in the range of 10^4 to 10^8 relative to the peak value at 0.55 MeV. The average neutron energy is about 1 MeV compared to 2 MeV for the fission spectrum. The plotted neutron spectra represent the neutrons leaving the target region, which account for the interactions between the high-energy spallation neutrons

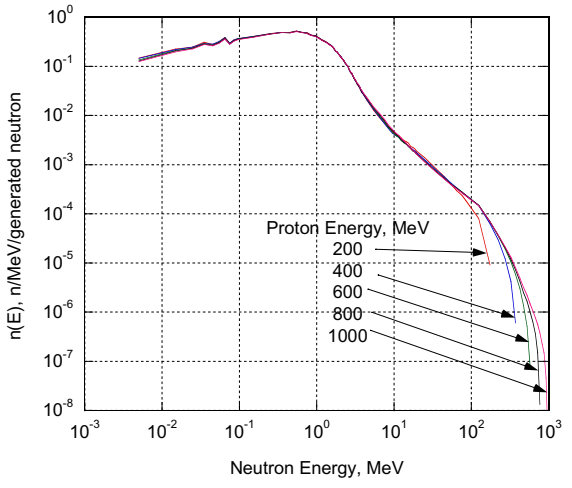

Fig. 7. Generated neutron spectra for different proton energies normalized per generated neutron.

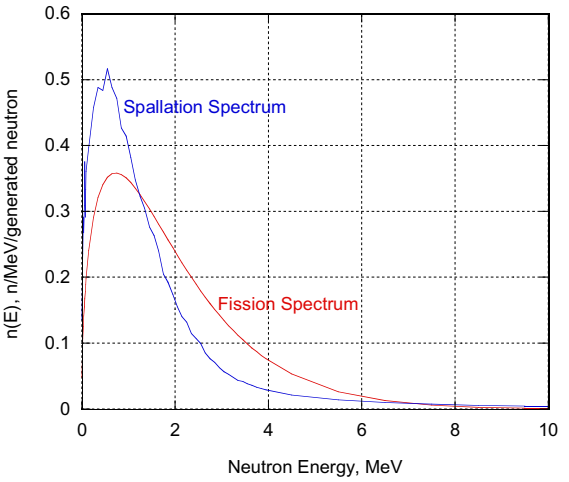

Fig. 8. Fission spectrum compared to the generated neutron spectra normalized per generated neutron.

and the LBE target material. These spectra include secondary neutrons from the (n,xn) interactions, and neutron slowing down through inelastic and elastic interactions. Fig. 8 shows both the generated neutron spectrum from Fig. 7 and the fission spectrum. The generated neutron spectrum is softer than the fission spectrum; however it has a very high-energy tail as shown in Fig. 7. This high-energy tail affects the nuclear responses in the structural material. It enhances the helium production rate, which affects the mechanical properties of the structural materials; further details are given in the buffer size section.

6. Beam window nuclear responses

As an example, the nuclear responses in the beam window are given in Table 1 for the 600 MeV protons and the beam current is normalized to 40 μA/cm^2. The energy deposition density in the HT-9 beam window is 766.5 W/cm^3 and the peak value in the LBE material is 796 W/cm^3 at 1.75 cm from the LBE surface. The gas production and the atomic displacement cross-sections used in the analyses do account for the nuclear responses generated by the protons and the neutrons [8]. In the beam window, the neutrons are responsible for 69% of the atomic displacement and the protons are generating more than 96% of the gas production rate. The high gas production rate affects the mechanical properties of the window material, which requires experimental data for realistic lifetime prediction of the structural material. Structural analysis [4] utilizing experimental data with lower helium per atomic displacement shows that the beam window may be able to operate for full power year with 40 μA/cm^2 current density.

Table 1
Target window nuclear responses from 600 MeV proton beam with 40 μA/cm^2 current density

Energy deposition, W/cm^3	766.49
Atomic displacement, dpa/y	
Neutrons	46.2
Protons	21.1
Total	67.3
Helium production, appm/fpy	
Low energy neutrons $\leqslant$ 20 MeV	5.7
High energy neutrons $>$ 20 MeV	50.2
Protons	1437.3
Total	1493.2
Hydrogen production, appm/fpy	
Low energy neutrons $\leqslant$ 20 MeV	6.3
High energy neutrons $>$ 20 MeV	1010.1
Protons	26,753.1
Total	27,769.5

7. Buffer requirement and impact on the neutron utilization

The analysis was performed as a function of the buffer thickness. The cross-section areas required for the inlet and the outlet LBE coolant channels define the minimum buffer thickness, which is 7 cm for 5 MW beam with 600 MeV protons [4–6]. The neutron yield (the total number of generated neutrons per proton leaving the target region) has a low sensitivity to the buffer thickness as shown in Fig. 9. The neutron yield reaches a saturation value at a buffer thickness of ~40 cm. The saturation value is about 1.14 times the value obtained with the 7-cm minimum buffer thickness. However, the number of neutrons utilized for material transmutation (the generated neutrons that reach the SCM) is significantly reduced as the buffer thickness is increased. This is also shown in Fig. 9 where the neutron utilization fraction drops from 0.71 with 7-cm buffer to 0.25 with 40-cm buffer. The axial neutron leakage is increased as the buffer thickness is increased. This requires the target design to reduce the buffer thickness as much as possible.

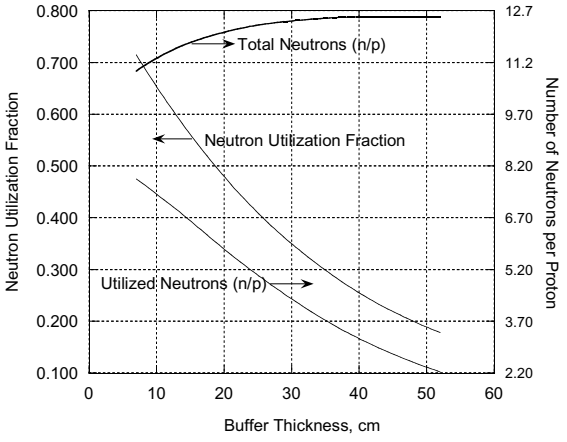

Fig. 9. Neutron utilization and neutron yield as a function of the buffer size for 600 MeV proton beam.

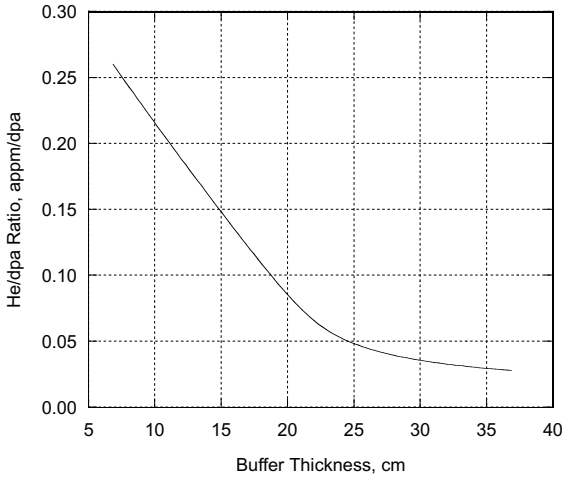

Fig. 10. Transmuter structure helium/atomic displacement ratio as function of the buffer thickness for 600 MeV proton beam.

The nuclear responses in the structural material at the outer buffer surface of a fast transmuter system change linearly with the reciprocal of the outer buffer radius [5]. The other important parameter for the structural material performance is the helium to atomic displacement ratio. Fig. 10 shows this ratio as a function of the buffer thickness for HT-9 alloy, which is in the range of 0.1–0.3 appm He/dpa. This ratio is about 0.26 for HT-9 in a typical fast reactor spectrum. For the above beam parameters with a fast transmuter, the results show that the 7-cm buffer thickness protects the structural material from the nuclear responses caused by the proton beam and the generated neutrons, utilizes most of the generated neutrons, and has adequate cross-section area for the inlet and the outlet LBE coolant channels. Therefore, the lifetime of the structural material around the buffer will depend on the operating temperature, the nuclear responses, and the loading conditions similar to fast fission systems.

8. Deuterons versus protons for neutron generation

Another characterization for the LBE material performance was performed with deuterons instead of protons. The deuteron energy was varied in the range of 200–1000 MeV similar to the proton characterization.

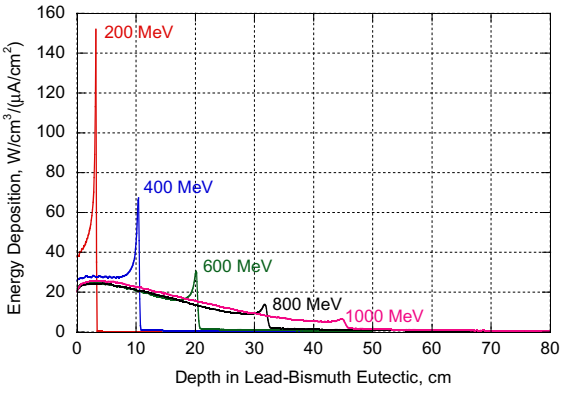

Fig. 11. Spatial energy deposition in the LBE for different deuteron energies.

The energy deposition profile in the LBE for different deuteron energies is shown in Fig. 11 and the results are normalized to the deuteron current density. The deuteron energy deposition profiles are similar to the proton profiles. However the range of the deuterons with energy E is about twice the range of the proton with energy $E/2$. Also, the peak energy deposition from the deuterons is about twice the corresponding value for the protons with same energy. This means that the neutrons are generated over shorter range, which has positive impact on the transmuters as will be discussed later and negative impact on the thermal hydraulics.

Similar to the proton case, the total energy deposition and the neutron production increase as the deuteron energy increases. The deuteron generates slightly more energy and neutrons than the proton of the same energy. In the energy range of 400–1000 MeV, the deuteron generates about 7–9% more neutrons relative to the proton. The deuteron has a shorter range, which increases the probability for the forward high-energy spallation neutrons to multiply through (n,xn) interactions and to slow down through elastic and inelastic interactions with LBE material. The resulting neutron spectrum is slightly softer because of these interactions. Fig. 12 shows the generated neutron distribution along the target buffer outer surface for different proton and deuteron energies, which shows the deuteron generating more neutrons than the proton with similar spatial distribution. However, there are other issues related to the use of deuterons including the accelerator cost, which require cost-benefit analyses to compare with proton case.

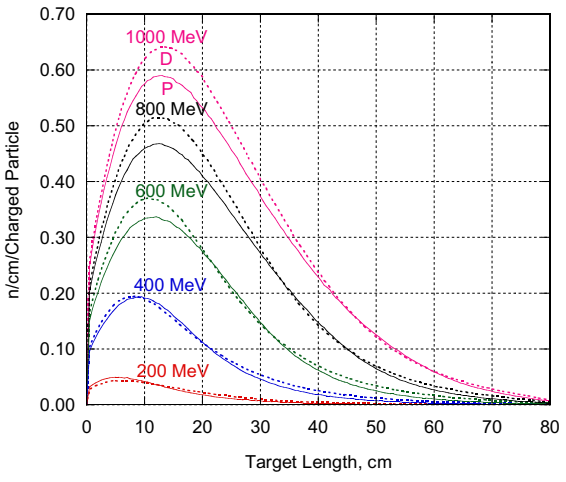

Fig. 12. Generated neutron distribution along the target buffer outer surface for different proton and deuteron energies.

9. Conclusions

The characterization results of LBE target material for accelerator driven transmuters presented in this paper reached the following main conclusions:

1. Increasing the charged particle energy reduces the peak power density and spreads the energy deposition in the lead–bismuth target material. Such effects reduce the maximum window temperature and facilitate the heat removal from the target.
2. The total energy deposition per generated neutron decreases fast as the charged particle energy increases up to ~600 MeV, then it decreases slowly.
3. The neutron yield increases with the energy of the charged particles. However the high-energy neutron ($E > 20$ MeV) fraction reaches a saturation value of about 5% of the total generated neutrons as the charged particle energy increases.
4. The uniformity of the generated neutron distribution increases in the beam direction as the energy of the charged particles increases. The peak value is always shifted away from the beam entry surface. Increasing the uniformity of the generated neutron distribution reduces the power peaking in the transmuter.
5. The high-energy neutrons ($E > 20$ MeV) have similar spatial distribution with more shifting for the peak value in the beam direction away from the beam entry surface.
6. The generated neutron spectrum does not change with the energy of the charged particles except for the upper end of the spectrum, which is 4–8 orders of magnitude less than the peak value.
7. The average energy of the generated neutrons with 7-cm LBE buffer is ~1 MeV compared to 2 MeV for fission neutron spectrum. However, the high-energy tail of the neutron spectrum affects the nuclear responses in the structural materials.
8. The use of lead–bismuth buffer with a small thickness, which is required for the inlet and outlet coolant

channels, reduces the nuclear responses in the structural material around the target to the observed values in the fast fission reactors.

9. The neutron balance analysis shows that the large buffer thickness reduces significantly the neutron utilization factor. For example, at 40-cm buffer thickness, the neutron utilization factor is 0.25, which means a beam power loss of 75%.
10. The range of the deuteron with energy E is about twice the range of the proton with energy $E/2$. Also, the peak energy deposition from the deuteron is about twice the corresponding value for the proton with same energy.
11. In lead–bismuth, deuterons produce slightly more neutrons than protons. For the same axial target length and beam particle energy, the difference is about 7–9% for the deuterons in the energy range of 400–1000 MeV. For deuterons, other issues including the beam generation cost require further analyses to judge the value of generating more neutrons per charged particle.

Acknowledgements

The submitted manuscript has been created by the University of Chicago as Operator of Argonne National Laboratory ('Argonne') under contract no. W-31-109-ENG-38 with the US Department of Energy. The US Government retains for itself, and others acting on its behalf, a paid-up, nonexclusive, irrevocable worldwide license in said article to reproduce, prepare derivative works, distribute copies to the public, and perform publicly and display publicly, by or on behalf of the Government.

References

[1] A. Dedoul, B. Gromov, E. Yefimov, E. Zemskov, K. Ivanov, M. Leonchuk, Yu. Orlov, D. Pankratov, Z. Sivack, V. Troyanov, N. Khaveyev, V. Chitaykin, V. Chekunov, N. Klimov, M. Koulikov, V. Stepanov, T. Kitano, M. Ono, Conceptual Design of Molten Lead–Bismuth Target Complex of Integral Type for ADS, Accelerator Applications/Accelerator Driven Transmutation Technology and Applications 01 (AccApp-ADTTA'01), Reno, Nevada, November 2001.

[2] J.U. Knebel, J.-C. Klein, D. Gorse, P. Agostini, F. Gröschel, P. Kupschus, T. Kirchner, J.-B. Vogt, MEGAPIE-TEST: A European Project on Spallation Target Testing, Accelerator Applications/Accelerator Driven Transmutation Technology and Applications 01 (AccApp-ADTTA'01), Reno, Nevada, November 2001.

[3] A. Dedoul, S. Grishakov, Ye. Yefimov, Ye. Zemskov, M. Leonchuk, D. Pankratov, D. Rachkova, Z. Sivak, V. Chitaykin, V. Chekunov, S. Sidorkin, F. Perekrestenko, V. Stepanov, N. Klimov, M. Kulikov, Concept of Lead–Bismuth Liquid Metal Target for Proton Accelerator of Moscow Meson Plant, Accelerator Applications/Accelerator Driven Transmutation Technology and Applications 01, AccApp-ADTTA'01, Reno, Nevada, November 2001.

[4] Y. Gohar, P. J. Finck, L. Krajtl, J.E. Herceg, W.D. Pointer, J. Saiveau, T. Sofu, A. L. Hanson, M. Todosow, M. Koploy, P. Mijatovic, Lead– Bismuth Target Design for the Subcritical Multiplier (SCM) of the Accelerator Driven Test Facility (ADTF), Argonne National Laboratory Report, ANL/TD/02-01, 2002.

[5] Y. Gohar, J. Herceg, L Krajtl, D. Pointer, J. Saiveau, T. Sofu, P. Finck, Lead–bismuth-Eutectic Spallation Neutron Source for Nuclear Transmuter, Accelerator Applications/Accelerator Driven Transmutation Technology and Applications 01 (AccApp-ADTTA'01), Reno, Nevada, November 2001.

[6] D. Pointer, T. Sofu, Y. Gohar, in: Proceedings of ASME FEDSM'02, 2002 ASME Fluids Engineering Division Summer Meeting, Montreal, Quebec, Canada, 14–18 July 2002.

[7] MCNPX Team, MCNPX Version 2.4.j, Los Alamos National Laboratory, LAUR02-2127, 25 March, 2002.

[8] E. Pitcher, Elemental Neutron- and Proton-Induced Displacement and Gas Production Cross-sections for Incident Particle Energies Ranging from 16 to 3120 MeV, paper presented at Accelerator Applications/Accelerator Driven Transmutation Technology and Applications 01 Meeting (AccApp-ADTTA'01), Reno, Nevada, November 2001; and Eric Pitcher, Private Communication, 2001.